PAPER

Improvement of work function and hole injection efficiency of graphene anode using CHF_3 plasma treatment

2D Materials

RECEIVED
29 September 2014

ACCEPTED FOR PUBLICATION
24 November 2014

PUBLISHED
31 December 2014

PAPER

Improvement of work function and hole injection efficiency of graphene anode using CHF_3 plasma treatment

Himchan Cho[1,5], Seong Dae Kim[2,5], Tae-Hee Han[1], Intek Song[3,4], Jin-Woo Byun[1], Young-Hoon Kim[1], Sungjoo Kwon[1], Sang-Hoon Bae[2], Hee Cheul Choi[3,4], Jong-Hyun Ahn[2] and Tae-Woo Lee[1]

[1] Department of Materials Science and Engineering, Pohang University of Science and Technology (POSTECH), Pohang 790-784, Korea
[2] School of Electrical and Electronic Engineering, Yonsei University, Seoul 120-749, Korea
[3] Center for Artificial Low Dimensional Electronic Systems, Institute for Basic Science (IBS), Pohang 790-784, Korea
[4] Department of Chemistry, Pohang University of Science and Technology (POSTECH), Pohang 790-784, Korea
[5] These authors equally contributed to this work.

E-mail: twlee@postech.ac.kr **and** ahnj@yonsei.ac.kr

Keywords: graphene, fluorination, hole injection efficiency, work function, hole-only device, dark injection space-charge-limited current transient measurement

Abstract

We report improvement of hole injection efficiency of a graphene anode by tuning its work function (WF) via surface fluorination. We used chemical vapor deposition to synthesize high-quality graphene sheets and then treated them with CHF_3 plasma to induce fluorination. We used x-ray photoelectron spectroscopy to examine the fluorine coverage and the kind of chemical bonds in fluorinated graphene (FG). Also, we used ultraviolet photoelectron spectroscopy to systematically study the changes in the WF and sheet resistance of the FG sheets with varying plasma exposure time (0, 10, 30, 60, 90 s) to find an optimum fluorination condition for hole injection. The WF of graphene sheets was increased by up to 0.74 eV, as a result of the formation of carbon-fluorine bonds that function as negative surface dipoles. We fabricated hole-only devices and conducted dark injection space-charge-limited-current transient measurement; the fluorination greatly increased the hole injection efficiency of graphene anodes (from 0.237 to 0.652). The enhanced hole injection efficiency of FG anodes in our study provides wide opportunities for applications in graphene-based flexible/stretchable organic optoelectronics.

1. Introduction

Graphene, a sp^2-hybridized two-dimensional (2D) carbon sheet, is a possible alternative electrode in electronics and optoelectronics because of its superior optical, electronic and mechanical properties such as very high optical transparency [1, 2], high charge carrier mobility [3–5], thermal conductivity [6] and flexibility [1, 2, 7]. Especially, graphene sheets grown by chemical vapor deposition (CVD) have enormous potential for use in flexible/stretchable organic light-emitting diodes (OLEDs) and organic solar cells (OSCs) as an alternative to indium tin oxide (ITO) electrodes because ITO is not a suitable electrode for flexible/stretchable devices due to its brittle nature, increasing material cost and possible diffusion of In and Sn atoms into overlying organic layers [1, 2].

However, the pristine graphene (PG) sheet has relatively higher sheet resistance R_{sh} ($>300\,\Omega\,sq^{-1}$) and lower work function (WF) (~4.4 eV) than those of ITO ($\sim 10\,\Omega\,sq^{-1}$, ~4.7 eV), and these demerits must be overcome to achieve uniform and efficient charge spreading and injection [1]. To reduce the R_{sh} of PG, charge-transfer doping with electron-withdrawing *p*-dopants such as HNO_3 and $AuCl_3$ is effective [1, 8, 9]. To increase the WF of PG, two approaches have generally been used: charge-transfer doping and surface functionalization. Charge-transfer doping by surface modification with electron-withdrawing *p*-dopants or electron-donating *n*-dopants can respectively either increase or decrease WF of PG by altering its Fermi energy [9–11]. Surface functionalization can create dipoles on the surface of PG; the dipoles can change WF of PG by facilitating or suppressing electron escape from the surface [12–14]. For

example, the formation of covalent bonds between carbon atoms and other atoms like fluorine and chlorine or molecules containing them onto PG can induce WF change of PG [12–14].

Surface functionalization of PG with fluorine provides a WF-increased graphene with high thermal stability and mechanical strength due to the large binding energy of carbon-fluorine bonds which makes the gain in cohesive energy per atom [15–17]. Also, the high chemical reactivity and electronegativity of fluorine can effectively modify electronic properties of PG [16, 17]. Fluorination of PG is usually achieved by exposing it to fluorine-containing gas or its plasma. Especially, plasma treatment can provide a simple, controllable and rapid way to fabricate fluorinated graphene (FG) at room temperature [13–15, 18–22]. However, although FG has a great potential as a 2D transparent conductor, only a few studies have reported its application in devices in the fields of dye-sensitized solar cells [19] and Li primary batteries [23]. Use of FG for electrodes of OLEDs and OSCs has not been reported. To apply FG to OLED/OSC devices, the fundamental studies on surface electronic structures on FG and their effect on hole injection to an overlying organic semiconducting layer in organic devices are imperative.

Here, we report the preparation and surface characterization of FG sheets and their enhanced hole injection capability as anodes in hole-only devices (HODs). We fabricated four-layer PG (4LPG) sheets on a poly(ethylene terephthalate) (PET) substrate by using CVD growth under optimized conditions and subsequent sequential poly(methyl methacrylate) (PMMA) transfer process, and then conducted CHF_3 plasma treatment to prepare functionalized 4LPG with fluorine. To maintain high conductivity of the 4LPG, the plasma treatment was conducted under an optimized process condition so that only the surface of the 4LPG could be fluorinated. To systematically analyze the surface bonding states of the 4LFG sheets and their optical and electronic properties we used x-ray and ultraviolet photoelectron spectroscopy (XPS and UPS), Raman spectroscopy, UV–visible spectroscopy (UV–vis). We also investigated how HNO_3 treatment affected the 4LFG sheets. Finally, we confirmed that the increased WF of the 4LFG sheets can greatly increase hole injection efficiency by fabricating HODs and performing dark-injection space-charge-limited current (DI SCLC) transient measurement, which is often used to estimate charge carrier injection efficiency into an organic film, and charge carrier mobility of the film.

2. Experimental details

2.1. Four-layer fluorinated graphene fabrication

Monolayer graphene sheet was synthesized using CVD on a Cu foil (25 μm thickness). A Cu foil was placed at the center of the quartz tube and the temperature of the furnace was increased to 1000 °C with a flow of H_2 gas at 8 sccm for 2.5 h at 110 mTorr. During graphene growth, CH_4 gas was supplied as a carbon source at a flow rate of 20 sccm at 300 mTorr for 1 h, while maintaining the H_2 flow rate. Finally, the furnace was cooled to room temperature while maintaining the H_2 flow rate at 8 sccm. After the synthesis of graphene on a Cu substrate, PMMA was spin-coated on top of the graphene to support it. Before etching the Cu substrate, graphene grown on its back side was etched away using a reactive ion etcher (RIE) (SNTEK, BCS5004) at 100 W for 10 s using O_2 gas at a flow rate of 20 sccm. The Cu substrate was etched using $FeCl_3$-based Cu etchant, CE-100 (Transene Company). The monolayer graphene sheet was transferred onto a transparent PET substrate. We chose 4LPG to obtain high conductivity enough for its use as anodes in HODs. To obtain 4LPG sheet, these processes were repeated four times without the fluorination step. The surface of the 4LPG sheet was fluorinated using the RIE at 20 W with various exposure times (0, 10, 30, 60, 90 s) using CHF_3 gas at a flow rate of 10 sccm at 85 mTorr.

2.2. XPS, UPS, Raman spectroscopy and UV–vis

XPS and UPS studies were conducted using an AXIS-Ultra DLD (Kratos Inc., UK). For XPS, a monochromatic Al-Kα line (1486.6 eV) was used with pass energies of 160 eV for survey and of 40 eV for narrow scan. For UPS, He I radiation (21.2 eV) was used with emission current of 10 mA and pass energy of 5 eV. Identification of PG and FG sheets transferred on Si wafers (300 nm thickness of SiO_2) were performed by Raman spectroscopy (UniNanotech, UniRAM-3500) using a laser with 532 nm wavelength. The transmittance of PET/4LPG and PET/4LFG samples was measured using a UV–vis spectrophotometer (Scinco S-3100) with the PET substrate as a reference.

2.3. HOD fabrication and characterization

A pre-patterned ITO anode on a glass substrate was sonicated with acetone and isopropyl alcohol in an ultrasonic bath, then boiled on a hot plate at 300 °C to evaporate the solvent quickly. A graphene sheet was HNO_3-treated and formed manually into a graphene anode pattern. The patterned graphene anode on a PET substrate, and a cleaned ITO anode were UV-ozone treated for 10 and 30 min, respectively. Then, a 70 nm thick poly(3,4-ethylenedioxythiophene):polystyrene sulfonate (PEDOT:PSS) layer was formed on the ITO anode by spin-coating as a hole injection layer. To ensure electrical contact, PEDOT:PSS on the edges of the ITO anode was removed using a mixture of deionized water and acetone, then the anode was immediately baked on a hot plate at 150 °C for 30 min. Then a 2.4 μm-thick hole transport layer of NPB and a 110 nm-thick cathode of aluminum were vacuum-

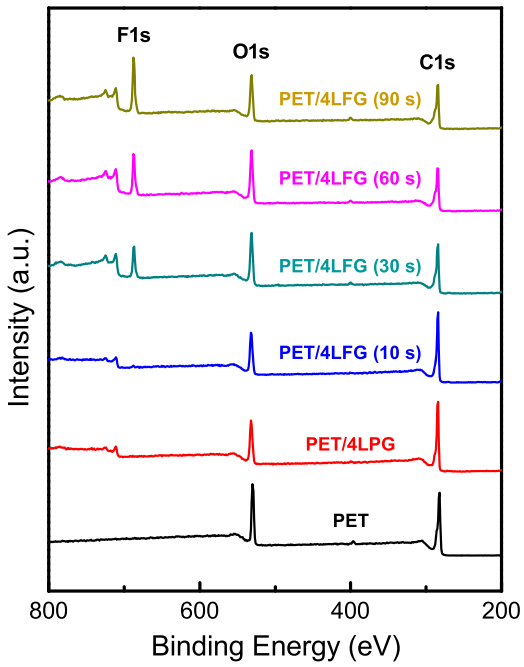

Figure 1. XPS survey spectra of a PET substrate, 4LPG and 4LFG on a PET substrate with varying plasma exposure time (10, 30, 60, 90 s). Peaks of C1s, O1s and F1s core electron states are labeled. Lines have been shifted vertically for clarity.

deposited in sequence on the prepared (i) Glass/ITO, (ii) Glass/ITO/PEDOT:PSS, (iii) PET/4LPG and (iv) PET/4LFG. The devices were encapsulated with a glass lid using an epoxy resin in a nitrogen atmosphere.

For current density-electric field (*J-E*) measurement, we used a computer-controlled source-measurement unit (Keithley 236) and a spectroradiometer (Minolta CS2000). For DI SCLC transient measurement, constant voltage pulse was applied to the devices by using a pulse generator (HP 214 B), and the output signal was monitored by an oscilloscope (Agilent Infiniium 54832B). All measurements were conducted under ambient conditions and room temperature.

3. Results and discussion

The fluorine coverage and the nature of chemical bonds of polyethylene terephthalate (PET) substrate, 4LPG and 4LFG sheets on PET substrates with plasma exposure time of 10, 30, 60 and 90 s, were examined by XPS (figure 1). The presence of strong O1s peak in all spectra, including bare PET, indicates that all of these O1s peaks are mainly due to oxygen moieties of PET. The continuous increase in F1s peak intensity after 10 s clearly demonstrates that the plasma treatment successfully fluorinated graphene (mainly after 10 s).

The change in chemical bonds of graphene with fluorination was investigated by analyzing individual C1s and F1s spectra (figures 2(a)–(d)). The C1s and F1s spectra were systematically de-convoluted into summations of Gaussian-Lorentzian curves. Fits were considered valid only if each fitting parameter (i.e. intensity, width, position) had p-value <0.01. In the C1s spectrum of a 4LPG sheet on the PET substrate (figure 2(b)), four different components (at 284.7, 285.3, 286.4 and 289.3 eV) were observed; we identified them as C=C (sp^2), C–C (sp^3), C=O and C(=O)O bonds, respectively [20, 24, 25]. When compared with the C1s spectrum of the pristine PET substrate (figure 2(a)), these peaks should be considered as the superposition of graphene and PET components; for instance, the sp^2 component was significantly increased after graphene transfer when compared with sp^3 counterpart. Fluorine-bonded carbon peaks, of which bonding energy >290 eV, were not detected.

The C1s and F1s spectrum of a 4LFG sheet on the PET substrate after 60 s of plasma treatment represents the emergence of various kinds of carbon-fluorine bonds (figures 2(c),(d)). The bonding energies of carbon atoms that are bound to fluorine atoms were observed at 286.7, 289.3, 291.5 and 293.6 eV (figure 2(c)). They were respectively assigned to C*-CF_n (secondary carbon to fluorine atoms), C-F, C-F_2 and C-F_3 bonds in good accordance with literatures [13, 21]. The spectrum at 286.7 eV should be considered as an overlap of C*-CF_n and C=O peaks, because their bonding energies are quite comparable to each other and the peak intensity is increased upon fluorination [21, 26, 27]. Similarly, the spectrum at 289.3 eV should be considered as an overlap of C-F and C(=O)O spectra [26, 27]. The incorporation of fluorine content into PG bends and distorts sp^2-hybridized carbon lattice with various bonding patterns [17, 28]. Especially, the carbon atoms bonded with two or three fluorine atoms can act as a termination group [28]; therefore, appearance of C-F_2 and C-F_3 peaks as well as increase in sp^3 intensity with respect to sp^2 peak imply that the graphene lattice may have been slightly damaged during the plasma treatment [21]; this damage is also suggested by the increases in in transmittance (figure 3(a)) and in R_{sh} (table 1). The transmittance of the 4LPG sheet was increased by ~2% after the plasma treatment (60 s of plasma treatment) within the wavelength range of visible light. This increase may be attributed to either the partial etching of the outermost layer of the 4LPG sheet or the transparent nature of carbon-fluorine bonds [22, 29]. Also, we attribute the increase in R_{sh} to both the insulating characteristic of sp^3-hybridized carbon atoms and the structural defects in the 4LFG lattice [18, 21]. The F1s spectrum of PET/4LFG (figure 2(d)) shows single Gaussian-Lorentzian components at 688.6 and 685.1 eV. The bonding state at 688.6 eV can be correlated to C-F bonds [18, 19, 21]. The smaller peak at the lower binding energy (685.1 eV) may be attributed to fluorine atoms that are bound to atoms with smaller electronegativity than carbon; a plausible candidate is Cu-F_2 bonding [21], because graphene may have been slightly contaminated by Cu remnants from the foil.

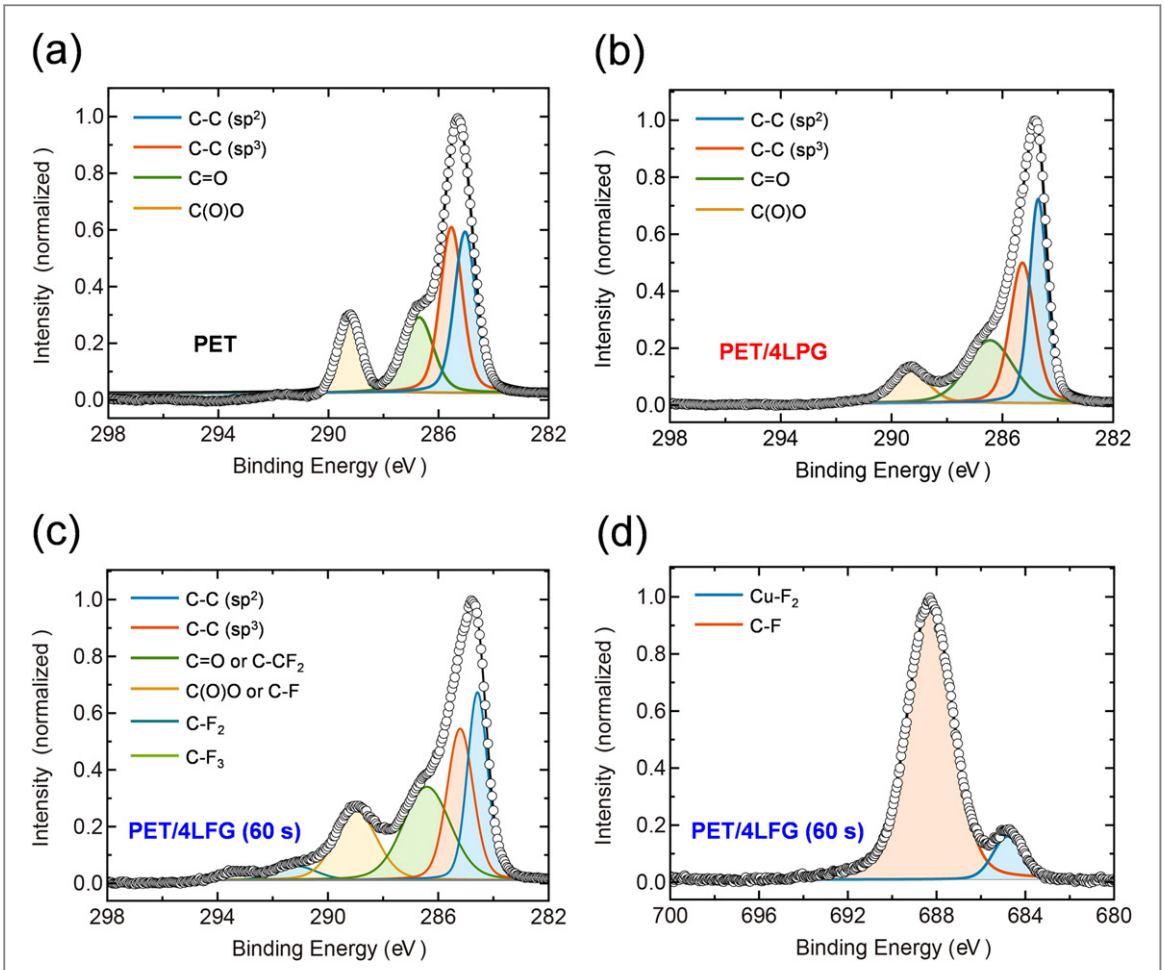

Figure 2. XPS C1s spectra of (a) a PET substrate, (b) 4LPG and (c) 4LFG (60 s of plasma treatment) on PET substrates. (d) XPS F1s spectrum of 4LFG on the PET substrate. Circles: spectrum before deconvolution.

Raman spectroscopy was used to identify 4LPG and 4LFG and to clarify their structural disorder. The Raman spectrum (figure 3(b)) of 4LPG showed G and 2D peaks at 1592 cm^{-1} and 2684 cm^{-1} respectively, and the I_{2D}/I_G ratio (~1.42) was consistent with the Raman data in layer-by-layer stacked CVD-grown multilayer graphene [8]. The D peak (at 1350 cm^{-1}) was very weak; this means that the 4LPG maintained high quality during transfer process [30]. In the 4LFG, the G and 2D peak positions and I_{2D}/I_G ratio were similar to those of 4LPG. However, the I_D/I_G ratio increased from 0.164 to 0.666, possibly due to the presence of fluorine moieties which generate sp^3-hybridized carbon atoms [31–33].

To investigate how much the fluorination reduced the hole injection barrier, we analyzed UPS spectra of 4LPG and 4LFG samples (plasma exposure time of 10, 30, 60 and 90 s) to measure their WFs (figures 3(c), (d)). The evolution of a shoulder peak at ~10.5 eV as plasma exposure time increased may demonstrate the presence of fluorine species because the peak arose from the photoelectrons emitted from fluorine 2p-like states (figure 3(c)) [13]. The WF can be obtained by subtracting the UPS spectrum width from the UV radiation energy (21.2 eV). The magnified UPS spectra around secondary electron cutoff (figure 3(d)) indicate that the secondary electron cutoff shifted gradually to lower energy as exposure time increased. This means that the WF of 4LPG gradually increased as the coverage of carbon-fluorine bonds increased: as the F1s/C1s peak ratio increased from 0 (0s) to 1.26 (90s), the WF of 4LPG also gradually increased from ~4.39 to ~5.13 eV. This gradual WF change can evidence the formation of carbon-fluorine bonds on the surface of 4LPG because the carbon-fluorine bonds can act as negative dipoles that increase WF [13, 14, 19]. HNO_3 treatment is an essential *p*-doping process to increase the conductivity of graphene sheets for fabrication of OLEDs with graphene anodes [1, 8]. Also, HNO_3 treatment can increase WF of graphene sheets [1, 8]. In accordance with the previously reported results [1, 8], we observed the reduction of R_{sh} of 4LFG after HNO_3 treatment (figure 4(a), table 1). To further investigate the effect of HNO_3 treatment on FG, we analyzed XPS and UPS spectra of PET/4LFG (60s of plasma treatment) after HNO_3 treatment. The sp^3/sp^2 carbon peak ratio increased from ~0.87 to ~1.32 in the C1s spectrum (figure 4(b)); this change implies that the HNO_3 treatment may change the hybridization of carbon atoms from sp^2 to sp^3 by

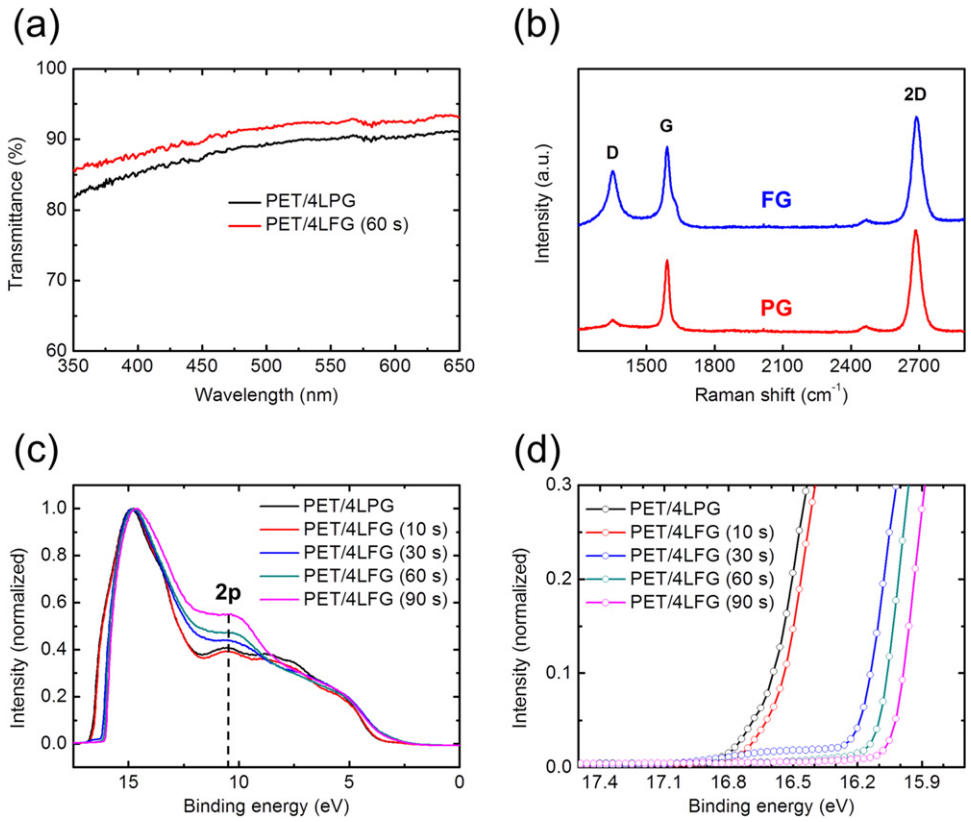

Figure 3. (a) Transmittance of 4LPG and 4LFG sheets (60 s of plasma treatment). (b) Raman spectra and (c) UPS spectra of 4LPG and 4LFG sheets (plasma exposure time of 10, 30, 60, 90 s). (d) Enlarged UPS spectra around secondary cutoff energy.

Table 1. F1s to C1s peak ratio in XPS spectra, WF and average sheet resistance (before and after HNO_3 treatment) of 4LPG and 4LFG with varying plasma exposure time (10, 30, 60, 90 s) on PET substrates.

		4LPG	4LFG (10 s)	4LFG (30 s)	4LFG (60 s)	4LFG (90 s)
F1s/C1s peak ^{ratio}			0.03	0.65	0.97	1.26
Work function $^{(eV)}$		4.39	4.43	4.95	5.06	5.13
Average sheet resistance $^{(\Omega\ sq-1)}$	Before HNO_3treatment	367	614	1040	1550	1930
	After HNO_3treatment	94.4	190	299	502	744

creating bonding between carbon atoms and other species [34]. Also, the small peak that corresponds to Cu-F_2 bonds at 685.1 eV (figure 2(d)) was not detected in the PET/4LFG sample after HNO_3 treatment (figure 4(c)). This absence may indicate that the Cu remnants in the 4LFG were totally removed by HNO_3, which is a well-known Cu etchant. The 0.14 eV reduction in the WF of 4LFG after HNO_3 treatment (from ~5.06 to ~4.92 eV) (figure 4(d)) supports this hypothesis that Cu remnants were removed, because removal of Cu-F_2 bonds reduces the number of surface dipoles on the 4LFG that can increase WF of graphene by restricting electron escape from its surface [13, 14].

To evaluate the hole injection capability of 4LFG, we fabricated 1,4-bis[(1-naphthylphenyl)amino] biphenyl (NPB)-based HODs that had a structure of X/NPB (2.4 μm)/Al (110 nm) where X is ITO, ITO/PEDOT:PSS (70 nm), PET/4LPG, or PET/4LFG (figure 5(a)). Using the SCLC model and the Poole-Frenkel equation, trap-free current in an organic film featuring ohmic contact is

$$J_{SCLC} = \frac{9}{8}\varepsilon_0\varepsilon_r\mu_0 \exp\left(\beta\sqrt{E}\right)\frac{E^2}{d}, \qquad (1)$$

where J_{SCLC} is the theoretical SCLC, ε_0 is the permittivity in vacuum, ε_r is the dielectric constant, μ_0 is the zero-field mobility, β is the Poole-Frenkel factor, E is the applied electric field and d is the thickness of the organic film [1, 35–38]. Therefore, hole injection efficiency of an HOD can be estimated by comparing J_{SCLC} to the current of the device. *J-E* characteristics of the HODs were compared to the calculated J_{SCLC} using equation (1) (figure 5(b)). To obtain a valid result, the comparison of current density was conducted in a trap-free region (figure 5(c)) [36]. The current density of HODs with ITO/PEDOT:PSS, PET/4LPG and PET/4LFG was close to J_{SCLC}, especially for PET/4LFG, whereas the current density of the HOD with ITO was

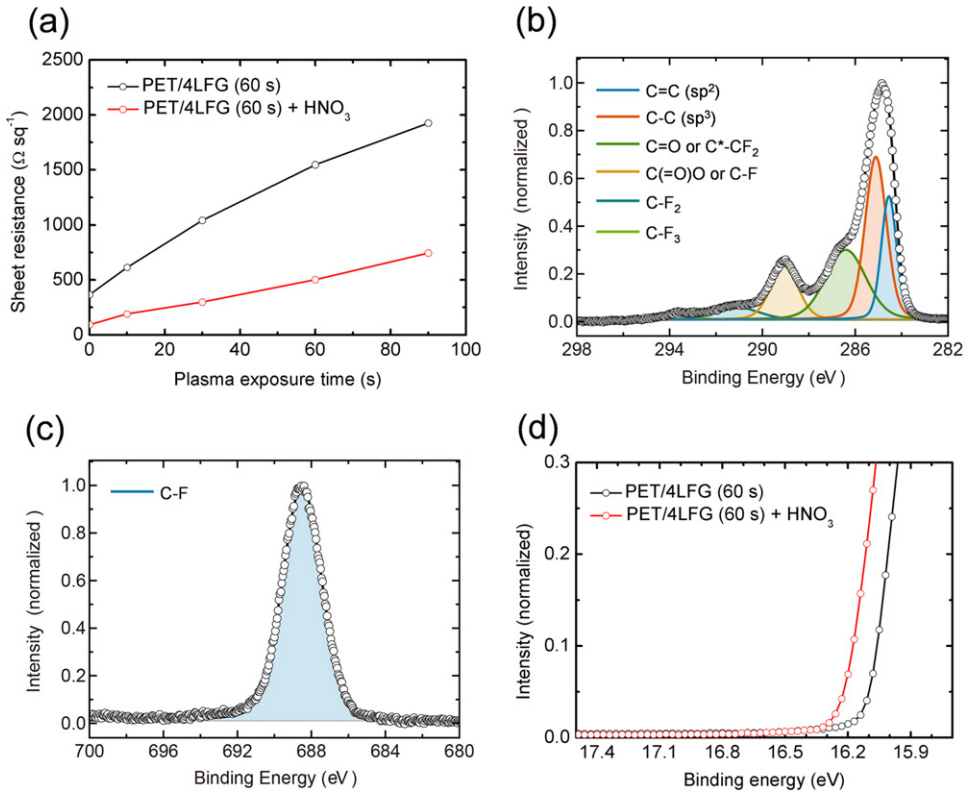

Figure 4. (a) Sheet resistance of 4LFG (60 s of plasma treatment) on PET substrates before and after HNO_3 treatment. XPS (b) C1s spectrum and (c) F1s spectrum of the 4LFG after HNO_3 treatment. (d) UPS spectra of the 4LFG before and after HNO_3 treatment.

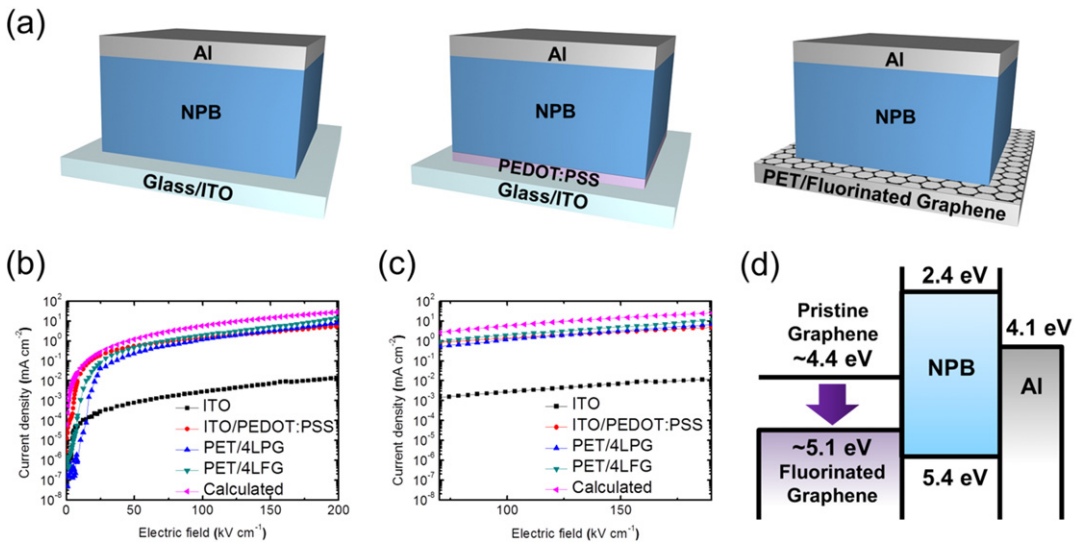

Figure 5. (a) Schematic diagrams describing HOD structures. (b) *J-E* characteristics of HODs with the calculated theoretical SCLC current. (c) Enlarged image of the *J-E* characteristics in the trap-free region. (d) Schematic energy level diagram of HODs with 4LPG and 4LFG anode.

smaller than J_{SCLC} by several orders of magnitude; this difference strongly indicates that the HOD with PET/4LFG exhibited higher hole injection efficiency than the other devices because of the reduced hole injection barrier in the HOD with PET/4LFG (figure 5(d)). The small current density of the HOD with ITO was attributed to large hole injection barrier between ITO and NPB.

To further understand the improvement of hole injection efficiency by fluorination, we conducted DI SCLC transient measurement. In the ideal case of ohmic contact and absence of traps, the transient current rapidly increases with applied voltage and reaches a temporal maximum of J_{DI} at $t = \tau_{DI}$ (figure 6(a)) [38–41]. This characteristic time corresponds to the time required for the fastest injected carriers to cross

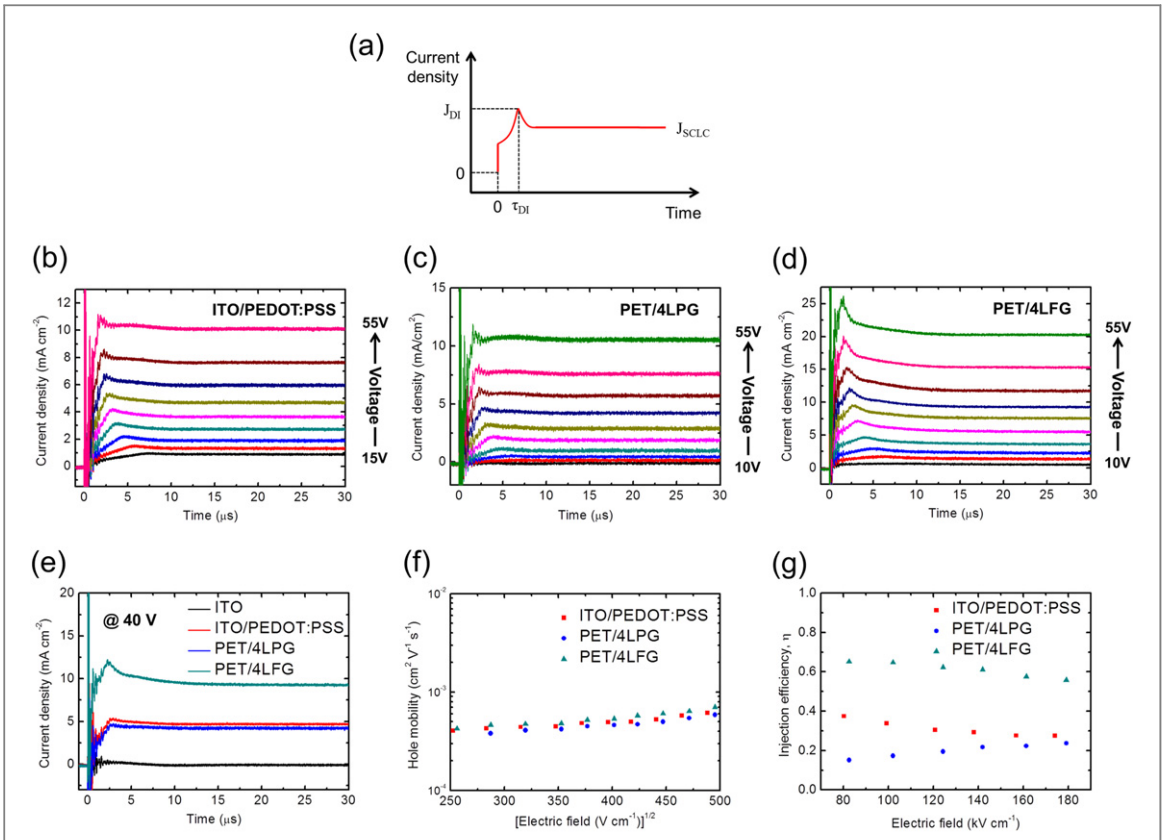

Figure 6. (a) Schematic diagrams of the ideal shape of a DI SCLC transient. DI SCLC transient of the HODs with (b) ITO/PEDOT:PSS, (c) PET/4LPG and (d) PET/4LFG at various applied voltages. (e) DI SCLC transient at 40 V of the HODs. (f) Hole mobilities and (g) hole injection efficiencies η of the HODs obtained by DI SCLC transient measurements.

the film. After $t = \tau_{DI}$, the current decreases until it reaches a steady state value of J_{SCLC}. Therefore, the emergence of a clear current transient peak in DI SCLC transient measurement can be a good indication of ohmic contact [38–42]. DI SCLC transient of the HODs with ITO/PEDOT:PSS, PET/4LPG and PET/4LFG (60 s of plasma treatment) at various voltages (figures 6(b)–(d)) all showed the typical trend of DI SCLC transients. The peak started to emerge at a voltage greater than a threshold, and τ_{DI} gradually shifted to shorter time with increasing voltage. However, although the HOD with PET/4LFG showed a clear and well-defined peak of J_{DI}, the HODs with ITO/PEDOT:PSS and PET/4LPG showed less-clear peaks; e.g., the current transient peak of the HOD with PET/4LFG was much stronger than that of others at the same voltage (figure 6(e)). The difference in clarity of the peaks strongly indicates that the ohmic contact was formed at the interface of 4LFG and NPB. The HOD with ITO showed very little current transient, and no current transient peak was observed, these observations correspond exactly to its *J-E* characteristics. However, although 4LPG had lower WF (~4.4 eV) than did ITO (~4.7 eV), the HOD with PET/4LPG exhibited a small current transient peak, which may originate from the WF increase of 4LPG during HNO_3 treatment.

We calculated the hole mobility of the HODs as

$$\mu_{DI} = \frac{0.787 d^2}{\tau_{DI} V}, \quad (2)$$

where V is the applied voltage [39–42], and plotted μ_{DI} of NPB in the HODs as a function of the square root of electric field (figure 6(f)). The calculated hole mobilities ranged from 4×10^{-4} to 6×10^{-4} cm^2 V^{-1} s^{-1}, which are in good agreement with the previously reported hole mobility from time-of-flight measurement [38]. Also, the hole injection efficiency of the HODs can be calculated as

$$\eta = \frac{J_{DI}}{1.2 J_{SCLC}} \quad (3)$$

where J_{DI} is the peak of the DI SCLC transient [1, 39–41]; when contact is ohmic, $J_{DI} \approx 1.2 J_{SCLC}$. The μ_0 and β values were extracted from the y-intercept and the slope of mobility-(electric field)$^{1/2}$ curves, respectively. The HODs with PET/4LFG exhibited much higher hole injection efficiency of ~0.6, with the maximum efficiency η_{max} of 0.652 (at 82.5 kV cm^{-1}) than did ITO/PEDOT:PSS ($\eta_{max} = 0.375$ at 80.2 kV cm^{-1}) and PET/4LPG ($\eta_{max} = 0.237$ at 179 kV cm^{-1}) (figure 6(g)). The hole injection efficiency of the HOD with ITO could not be calculated due to the absence of a current transient peak.

Therefore, we conclude that the increased WF of 4LFG greatly contributed to the improvement of its hole injection capability.

4. Conclusion

We conducted a systematic multi-stage study including FG preparation, surface characterization and HOD fabrication to analyze the changes in surface electronic structure and hole injection efficiency of FG as an anode. We synthesized PG sheets by an optimized CVD growth process and functionalized them by CHF_3 plasma treatment. The formation of carbon-fluorine bonds on the FG sheets was confirmed by systematically comparing XPS, UPS and Raman spectra of FG sheets with those of PG sheets. The gradual WF increase (by up to 0.74 eV) with respect to longer plasma exposure time was measured by analyzing UPS spectra. Using the FG sheets as anodes in HODs, we achieved significant enhancement in hole injection efficiency of a graphene anode (η_{max} increased from 0.237 to 0.652). This increase implies that fluorination of a graphene anode is an effective way to facilitate hole injection into an organic semiconducting layer in graphene-based flexible/stretchable OLEDs and OSCs.

Acknowledgments

This work was supported by the MSIP (Ministry of Science, ICT and Future Planning), Korea, under the 'IT Consilience Creative Program' (NIPA-2014-H0201-14-1001) supervised by the NIPA (National IT Industry Promotion Agency). This work was also supported by the National Research Foundation of Korea(NRF) grant funded by the Korea government (MSIP) (NRF-2012R1A2A1A03006049).

References

[1] Han T-H, Lee Y, Choi M-R, Woo S-H, Bae S-H, Hong B H, Ahn J-H and Lee T-W 2012 *Nat. Photon.* **6** 105
[2] Kim H, Bae S-H, Han T-H, Lim K-G, Ahn J-H and Lee T-W 2014 *Nanotechnology* **25** 014012
Kim M, An H, Lee W-J and Jung J 2013 *Electron. Mater. Lett.* **9** 517
Kim H, Kim E, W-J and Jung J 2013 *Electron. Mater. Lett.* **9** 417
[3] Hwang E H, Adam S and Sarma S D 2007 *Phys. Rev. Lett.* **98** 186806
[4] Bolotin K I, Sikes K J, Jiang Z, Klima M, Fudenberg G, Hone J, Kim P and Stormer H L 2008 *Solid State Commun.* **146** 351
[5] Xu W, Seo H-K, Min S-Y, Cho H, Lim T-S, Oh C, Lee Y and Lee T-W 2014 *Adv. Mater.* **26** 3459
[6] Wei N, Xu L, Wang H-Q and Zheng J-C 2011 *Nanotechnology* **22** 105705
[7] Verma V P, Das S, Lahiri I and Choi W 2010 *Appl. Phys. Lett.* **96** 203108
[8] Bae S *et al* 2010 *Nat. Nanotechnol.* **5** 574
[9] Xu W, Lim T-S, Seo H-K, Min S-Y, Cho H, Park M-H, Kim Y-H and Lee T-W 2014 *Small* **10** 1999
[10] Kwon K C, Choi K S and Kim S Y 2012 *Adv. Funct. Mater.* **22** 4724
[11] Leung T C, Kao C L, Su W S, Feng Y J and Chan C T 2003 *Phys. Rev.* B **68** 195408
[12] Şahin H and Ciraci S 2012 *J. Phys. Chem.* C **116** 24075
[13] Sherpa S D, Paniagua S A, Levitin G, Marder S R and Williams M D 2012 *J. Vac. Sci. Technol.* B **30** 03D102
[14] Sherpa S D, Levitin G and Hess D W 2012 *Appl. Phys. Lett.* **101** 111602
[15] Craciun M F, Khrapach I, Barnes M D and Russo S 2013 *J. Phys.: Condens. Matter* **25** 423201
[16] Dos S R B, Rivelino R, Mota F D B and Gueorguiev G K 2012 *J. Phys. Chem.* A **116** 9080
[17] Gueorguiev G K, Goyenola C, Schmidt S and Hultman L 2011 *Chem. Phys. Lett.* **516** 62
[18] Ho K-I, Liao J-H, Huang C-H, Hsu C-L, Zhang W, Lu A-Y, Li L-J, Lai C-S and Su C-Y 2014 *Small* **10** 989
[19] Das S, Sudhagar P, Verma V, Song D, Ito E, Lee S Y, Kang Y S and Choi W 2011 *Adv. Funct. Mater.* **21** 3729
[20] Felten A, Eckmann A, Pireaux J-J, Krupke R and Casiraghi C 2013 *Nanotechnology* **24** 355705
[21] Wang B, Wang J and Zhu J 2014 *ACS Nano* **8** 1862
[22] Robinson J T *et al* 2010 *Nano Lett.* **10** 3001
[23] Damien D, Sudeep P M, Narayanan T N, Anantharaman M R, Ajayan P M and Shaijumon M M 2013 *RSC Adv.* **3** 25702
[24] Park S, An J, Piner R D, Jung I, Yang D, Velamakanni A, Nguyen S T and Ruoff R S 2008 *Chem. Mater.* **20** 6592
[25] Xu Y, Bai H, Lu G, Li C and Gaoquan S. 2008 *J. Am. Chem. Soc.* **130** 5856
[26] Nansé G, Papirer E, Fioux P, Moguet F and Tressaud A 1997 *Carbon* **35** 175
[27] Gelius U, Hedén P F, Hedman J, Lindberg B J, Manne R, Nordberg R, Nordling C and Siegbahn K 1970 *Phys. Scr.* **2** 70
[28] Goyenola C, Stafström S, Schmidt S, Hultman L and Gueorguiev G K 2014 *J. Phys. Chem.* C **118** 6514
[29] Wang Z, Wang J, Li Z, Gong P, Liu X, Zhang L, Ren J, Wang H and Yang S 2012 *Carbon* **50** 5403
[30] Ferrari A C *et al* 2006 *Phys. Rev. Lett.* **97** 187401
[31] Graf D, Molitor F, Ensslin K, Stampfer C, Jungen A, Hierold C and Wirtz L 2007 *Nano Lett.* **7** 238
[32] Ferrari A C 2007 *Solid State Commun.* **143** 47
[33] Withers F, Dubois M and Savchenko A K 2010 *Phys. Rev.* B **82** 073403
[34] Das S, Sudhagar P, Ito E, Lee D, Nagarajan S, Lee S Y, Kang Y S and Choi W 2012 *J. Mater. Chem.* **22** 20490
[35] Choi M-R *et al* 2011 *ChemSusChem* **4** 363
[36] Siegrist T, Kloc C, Schön J H, Batlogg B, Haddon R C, Berg S and Thomas G A 2001 *Angew. Chem. Int. Ed.* **40** 1732
[37] Choi M-R, Han T-H, Lim K-G, Woo S-H, Huh D H and Lee T-W 2011 *Angew. Chem. Int. Ed.* **50** 6274
[38] So S K, Tse S C and Tong K L 2007 *J. Disp. Technol.* **3** 225
[39] Campbell A J, Bradley D D C and Antoniadis H 2001 *J. Appl. Phys.* **89** 3343
[40] Poplavskyy D, Su W and So F 2005 *J. Appl. Phys.* **98** 014501
[41] Tse S C, Tsang S W and So S K 2006 *J. Appl. Phys.* **100** 063708
[42] Small C E, Tsang S-W, Kido J, So S K and So F 2012 *Adv. Funct. Mater.* **22** 3261